Fullerene-based one-dimensional crystalline nanopolymer formed through topochemical transformation of the parent nanowire

Junfeng Geng,[1,*] Ilia A. Solov'yov,[2,3,†] David G. Reid,[1] Paul Skelton,[1] Andrew E. H. Wheatley,[1] Andrey V. Solov'yov,[2,3] and Brian F. G. Johnson[1]

[1]*Department of Chemistry, University of Cambridge, Cambridge CB2 1EW, United Kingdom*

[2]*Frankfurt Institute for Advanced Studies, Goethe University, Ruth-Moufang-Str. 1, 60438 Frankfurt, Germany*

[3]*A. F. Ioffe Physical-Technical Institute, Politechnicheskaya 26, 194021 St. Petersburg, Russia*

(Received 24 November 2009; revised manuscript received 11 March 2010; published 17 June 2010)

Large-scale practical applications of fullerene (C_{60}) in nanodevices could be significantly facilitated if the commercially available micrometer-scale raw C_{60} powder were further processed into a one-dimensional nanowire-related polymer displaying covalent bonding as molecular interlinks and resembling traditional important conjugated polymers. However, there has been little study thus far in this area despite the abundant literature on fullerene. Here we report the preparation and characterization of such a C_{60}-based polymer nanowire, $(\text{-}C_{60}\text{TMB-})_n$, where TMB=1,2,4-trimethylbenzene, which displays a well-defined crystalline nanostructure, exceptionally large length-to-width ratio and excellent thermal stability. The material is prepared by first growing the corresponding nanowire through a solution phase of C_{60} followed by a topochemical polymerization reaction in the solid state. Gas chromatography, mass spectrometry and ^{13}C nuclear magnetic resonance evidence is provided for the nature of the covalent bonding mode adopted by the polymeric chains. Theoretical analysis based on detailed calculations of the reaction energetics and structural analysis provides an in-depth understanding of the polymerization pathway. The nanopolymer promises important applications in biological fields and in the development of optical, electrical, and magnetic nanodevices.

DOI: 10.1103/PhysRevB.81.214114 PACS number(s): 81.07.−b, 81.10.Aj, 61.46.Km, 62.23.St

I. INTRODUCTION

Two important forms of carbon, fullerene (C_{60}) and carbon nanotubes, are closely related to each other by the structural commonality of their sp^2 frameworks. Carbon nanotubes have been widely investigated for the last decade, or so, as one-dimensional (1D) nanomaterials.[1–3] In contrast, fullerene 1D nanostructures, such as C_{60} nanowires, presently represent laboratory curiosities.[4–7] C_{60} nanowires are potentially very interesting nanomaterials because of the physical properties associated with their high surface area, low-dimensionality, and quantum-confinement effects.[8,9] It is also expected that, in contrast to their parent nanowires or individual fullerene building blocks, polymerized C_{60} nanowires will exhibit remarkably different and/or improved physical properties owing to the formation of polymeric chains and interchain cross-linking networks. From an application point of view, a major advantage of such polyfullerenes would be their biocompatibility as they are totally free of metal. This clearly contrasts to the case of carbon nanotubes, the growth of which is catalyzed by metal nanoparticles, and from which by no means all the metal can be removed by post-purification processes.[10] In this respect, C_{60} polymer nanowire could be biologically more attractive than carbon nanotubes for uses in, for example, drug delivery and biosensor preparation.[11–14] Additionally, C_{60} 1D nanopolymers are conjugated or nearly conjugated materials that promise outstanding photoelectrical properties because of the large magnitude of the nonlinear optical response of C_{60} and its excellent photoinduced charge-transfer behavior.[8] As such, they promise applications as optical limiters and photoconductors for solar-energy devices, fuel cells, and field-emission transistors.[15–22] All this makes C_{60} 1D nanopolymers important materials for further study.

Fundamental to the development of these materials is the question of how to make a metal-free, C_{60}-based 1D nanopolymer? In seeking to answer this question, we note first that a limited number of polymerization reactions of C_{60} have been reported in the literature.[23–31] For example, it has been shown that the polymerization of thin solid films of C_{60} may occur upon irradiation with visible-UV light. In this case, the thin films were prepared by vacuum deposition of pure C_{60} on a substrate.[23] On the basis of Raman scattering studies, such polymerization has been hypothesized to result from a [2+2] cycloadduction linkage between adjacent C_{60} molecules in the structure.[23,24] Single crystals of KC_{60}, prepared by the coevaporation of K and C_{60}, have undergone polymerization via formation of the same [2+2] structure motif but the whole polymer is a linear polyanion network, as suggested by electron-spin-resonance measurements, pointing to a possible donation of electrons from K atoms to the polymer chains.[25] An in-chain metal-fullerene $(\text{-}PdC_{60}\text{-})_n$ polymer, synthesized by the reaction of C_{60} with a palladium complex, $Pd_2[(C_6H_5CH{=}CH)_2C{=}O]{\cdot}CHCl_3$ has been noted.[26] Moreover, side-chain C_{60} copolymers formed through the attachment of C_{60} to an amino polymer substrate have also been reported with the coupling of C_{60} to the amino polymer being analogous to that observed for amines.[27,28]

The polymerization of C_{60} and C_{70} induced by moderately high pressures and high temperatures has also been reported.[29–31] In the case of C_{60}, new structural phases such as rhombohedral and tetragonal lattices may be formed, depending on the pressure and temperature employed.[29,30] These new phases are metastable at room temperature and pressure, and they can be understood in terms of a long-range ordered polymerization of C_{60} through cycloaddition reactions at the shorter intermolecular distances.[30] For C_{70},

the polymeric phase was obtained by treatment of hexagonally packed C_{70} single crystals under moderate hydrostatic pressure (2 GPa) at elevated temperature (300 °C).[31] The polymeric zigzag chains that extend along the *c* axis of the parent structure were suggested by single-crystal x-ray diffraction data while solid-state nuclear magnetic resonance and Raman measurement provide evidence for covalent chemical bonding between the C_{70} cages.

It has been demonstrated that crystallization of C_{60} molecules from organic solvents yields C_{60} nanocrystals with varied shapes and structures, and that these shapes and structures are dependent upon the crystallization conditions and the solvent(s) employed.[32–34] One example is the preparation of C_{60} nanowhiskers with a claimed face-centered-cubic structure using a liquid-liquid interface method.[35] This method has also been extended to prepare the nanowhiskers of C_{70}, iodine-doped C_{60}, and the C_{60}-based complex of $(\eta^2\text{-}C_{60})Pt(PPh_3)_2$.[35,36] In the second example, crystallization of C_{60} molecules from a 1,2,4-trimethylbenzene (1,2,4-TMB) solution of C_{60} has been found to be able to produce exceptionally long C_{60} nanowires under appropriate conditions, with a length-to-width aspect ratio as large as 3000, and an orthorhombic nanostructure.[37–39] In spite of these literature reports, however, it is clear that there has been little study of the synthesis of C_{60} polymer nanowire. This new class of 1D polymer is expected to exhibit similarities in structure to other conventionally important conjugated polymers such as polyacetylenes, polyanilines, and polyphenylenes while having distinguishing physical properties due to the unique molecular structure of C_{60}, the low dimensionality of the material and the crystalline nature of the network.

Here we report the preparation and characterization of a C_{60}-based polymer nanowire, $(\text{-}C_{60}TMB\text{-})_n$, which is formed when polymerization occurs in the corresponding parent nanowires via a topochemical solid-state reaction. The reactive monomers are preorganized in the crystalline unit cell at a distance commensurate with the repeat distance in the final polymer. In order to understand the polymerization pathway, we have employed gas chromatography (GC), mass spectrometry (MS), and ^{13}C nuclear-magnetic-resonance (NMR) spectroscopy to investigate the nature of the bonds formed during the polymerization process. Additionally, in order to explain the polymerization mechanism in more detail we have theoretically analyzed the associated molecular orientations, structural arrangements, and the favorable reaction pathways.

II. EXPERIMENTAL DETAILS

GC-MS analysis was carried out using a Perkin Elmer Turbomass GC-MS. This system utilizes an Autosystem XL GC connected to a small quadrupole mass analyzer. Samples were dissolved in CCl_4 prior to analysis and were introduced to the system using a split injection technique. After a delay of 1 min the mass spectrometer scan was initiated with the parameters set out below.

GC conditions: injection volume, 0.5 μl; injection temperature, 200 °C; helium-carrier gas pressure, 40ψ. Column: Perkin Elmer Elite PE-5MS (5% phenyl, 95% methyl polysiloxane); length, 30 m; ID, 0.25 mm; and film thickness, 0.25 μm. Column gradient: start temperature, 60 °C, for 1 min then ramped at 10 °C/min to 200 °C, which temperature was maintained for 2 min. Total analysis time was 17 min.

MS conditions: ionization mode, EI+; ionization energy, 70 eV; source temperature, 200 °C; transfer line temperature, 200 °C; mass range scanned, 50–650 Da; scan time, 0.5 s; interscan time, 0.1 s; and solvent delay time, 1 min.

^{13}C-NMR spectra were acquired at 100.62 MHz on Bruker AVANCE 400 standard bore (liquid state) and wide bore (solid state) spectrometers with standard Bruker broadband tuneable probes. Samples for solid-state NMR spectroscopy were packed into 4-mm zirconia rotors padded with polytetrafluoroethylene tape to take up excess space due to limited sample volumes. Relevant spectral acquisition parameters were as below.

Solution-state NMR spectra were obtained using pulse acquire with 10 s $\pi/2$ pulses, a recycle delay of 5 s, and broadband ^1H decoupling, and referenced relative to tetramethylsilane at 0 ppm. Solid-state NMR spectra were acquired with standard cross-polarization magic-angle spinning (CP-MAS) (12.5 kHz, 2.5 μs ^1H pulse, ramped CP time 5 ms, recycle delay 1 s) and high-power broadband ^1H decoupling during acquisition (fullerene nanowires). Pure fullerene was observed using direct polarization MAS (5 ms $^{13}C\pi/2$ pulse, recycle delay 60 s). Chemical shifts are referenced to the methylene carbon signal of glycine at 43.1 ppm which is back referenced to tetramethylsilane.

Transmission electron microscopy (TEM) and selected area electron diffraction (SAED) were performed using a JEOL JEM-3010× microscope operated at 300 kV and a JEOL 200CXi microscope operated at 200 kV, respectively. Specimens were directly deposited on copper grids coated with holey carbon films without any prior suspension treatment in solution.

Scanning electron microscopic (SEM) examinations were performed using a LEO-32 electron microscope operated at 5 kV. Samples were directly deposited on a specimen holder (carbon mat) without surface coating of a conducting material.

Raman spectroscopic studies were performed using a micro-Raman spectrometer with incident Ar ion laser at $\lambda = 514.5$ nm and RENISHAW software. Extra care was taken to avoid laser damage to the samples. To ensure this, the laser power employed was kept as low as possible and optical microscopic examinations were carried out for the nanowires before and after each measurement.

III. THEORETICAL METHODS

The structure and properties of the molecules involved in the nanowire polymerization process were studied theoretically. The calculations were performed with the GAUSSIAN 03 software package,[40] within the framework of the *ab initio* density-functional theory (DFT), which was successfully applied for the study of various nanoscaled systems (see, e.g., Refs. 41–46 and references therein). DFT is a common tool with which to calculate the properties of quantum many-

body systems in which many electron correlations play a role. The DFT formalism is well known and can be found in many textbooks (see, e.g., Refs. 47 and 48). Therefore in our work we present only the basic equations and ideas of this method.

Electronic wave functions and energy levels within the framework of DFT are obtained from the Kohn-Sham equations, which read as (see, e.g., Refs. 47 and 48)

$$\left(\frac{\hat{p}^2}{2} + \hat{U}_{ions} + \hat{V}_H + \hat{V}_{xc}\right)\psi_i = \varepsilon_i \psi_i, \quad i = 1, \ldots, N, \tag{1}$$

where the first term represents the kinetic energy of the ith electron with the wave function ψ_i and the energy ε_i, $\hat{U}_{ions}$ describes the electron attraction to the ionic centers, $\hat{V}_H$ is the Hartree part of the interelectronic interaction,[49] and $\hat{V}_{xc}$ is the local exchange-correlation potential.

The exchange-correlation potential is defined as a functional derivative of the exchange-correlation energy functional

$$\hat{V}_{xc} = \frac{\delta E_{xc}[\rho]}{\delta \rho(\vec{r})}. \tag{2}$$

Here ρ is the electron density. Equation (2) is exact and follows from the Hohenberg theory.[50] However, no unique potential E_{xc}, universally applicable for different systems and conditions, has been found so far. Approximate functionals employed by the DFT usually partition the exchange-correlation energy into two parts, referred to as the *exchange* and the *correlation* terms

$$E_{xc}[\rho] = E_x(\rho) + E_c(\rho). \tag{3}$$

Both terms are functionals of the electron density, which can be of two distinctly different types: either a *local* functional depending only on the electron density ρ or a *gradient-corrected* functional, depending on both ρ and its gradient, $\nabla\rho$. A variety of exchange-correlation functionals can be found in the literature. In our work we have used the hybrid Becke-type three-parameter exchange functional,[51] paired with the gradient-corrected Lee, Yang, and Parr correlation functional (*B3LYP*).[52,53]

In the calculations we accounted for all electrons in the system, and employed the standard STO-3G, 6-21G and 6-31G(d) basis sets.[54] The STO-3G and 6-21G basis sets were used for geometry optimization and energy calculation while the 6-31G(d) was used for simulating the nuclear magnetic-resonance properties. The semiempirical Austin model 1 (AM1) method[55,56] was also used to study the polymerization reaction energies. This method is based on Hartree-Fock formalism but includes many parameters obtained from empirical data. The AM1 method is significantly faster than the *ab initio* DFT method because it does not explicitly include the computationally time-demanding two-electron part of the Hamiltonian.

We have calculated chemical shielding tensors for different molecules of interest and compared the results with experimental measurements. According to NMR theory, the chemical shielding tensor can be computed as the second derivative of the electronic energy E with respect to the external magnetic field $\vec{B}$ and the nuclear magnetic moment of interest $\vec{m}^N$

$$\sigma_{ji}^N = \left(\frac{d^2E}{dB_i dm_j^N}\right)_{\vec{B},\vec{m}^N=0}. \tag{4}$$

Indices i and j correspond to the ith and jth components of the vectors $\vec{B}$ and $\vec{m}^N$, respectively. The gauge-origin problem inherent to finite basis-set calculations of NMR shieldings can be solved by using gauge-including atomic orbitals.[57–60]

The chemical shielding tensor σ_{ji} in Eq. (4) can be diagonalized to yield a tensor with three principal components, $\sigma_{11} \leq \sigma_{22} \leq \sigma_{33}$, which define the isotropic shielding as follows:

$$\sigma_{iso} = \frac{\sigma_{11} + \sigma_{22} + \sigma_{33}}{3}. \tag{5}$$

Isotropic shielding is an important quantity, because in a solution NMR experiment, rapid tumbling of the molecules commonly averages the chemical shielding tensor, and only the isotropic chemical shielding is detected. In solid samples, the presence of chemical shielding anisotropy often generates broad powder patterns, but in this case the MAS technique can be used to partially or completely average the chemical shielding anisotropy of powder patterns.

Another important quantity is the chemical shift δ, which is defined as the difference in shielding between the nucleus in the species under investigation, σ_s, and the shielding of the same nucleus in a reference compound, σ_{ref}

$$\delta(\text{ppm}) = 10^6 \times \frac{\sigma_{ref} - \sigma_s}{1 - \sigma_{ref}} \approx 10^6 \times (\sigma_{ref} - \sigma_s). \tag{6}$$

The approximation in Eq. (6) is often used because usually $\sigma_{ref} \ll 1$. This equation gives the chemical shift in parts per million (ppm). In this work, we are interested of the chemical shifts for the ^{13}C nuclei, which we have calculated relative to the chemical shift of the carbon atoms in tetramethylsilane.

IV. RESULTS AND DISCUSSION

A. Synthesis and characterization by GC-MS

Synthesis of the fullerene polymer nanowire required that we first prepared C_{60} nanowires using a 1,2,4-TMB solution of C_{60} by a previously described method.[37] We noted that the resulting nanowires were highly stable, as indicated by the fact that there was no detectable alteration in either their crystalline morphology, crystal color, or sample weight as a function of time. However, the solubility of the material was found to change with time. Unlike raw C_{60} powder, well known to be highly soluble in aromatic solvents, the as-made nanowires were only partially soluble in these solvents, and this solubility decreased further with time. After aging for a period of ~10 months, the nanowires became totally insoluble in common organic solvents including benzene, toluene, 1,2,4-TMB, and carbon tetrachloride. This initial obser-

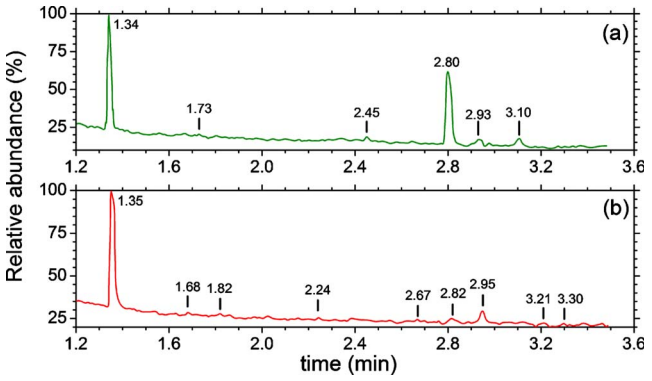

FIG. 1. (Color online) GC analysis of the C_{60}TMB nanowires. (a) GC analysis of the as-prepared sample. (b) GC profile of the aged sample. The GC peaks at 1.34 min in (a) and 1.35 min in (b) are attributable to the remnant of CCl_4 solvent, and the peaks at 2.93 or 2.95 min in the spectra are due to an impurity present in the system.

vation led us to speculate that a polymerization reaction might have occurred within the system, and that this had led to interesting physical and chemical properties, including excellent thermal stability and solvent-resistant behavior.

Observation of the loss of solubility was consistent with the results obtained from the GC-MS analysis. Tests were carried out using two suspensions of the solid in CCl_4, corresponding, respectively, to as-made and aged nanowires. Prior to the tests, the solids were resident in the solvent for 5 days. The results are shown in Fig. 1. As can be seen, GC successfully isolated 1,2,4-TMB molecules from the suspension containing the as-made nanowires, as indicated by the signals at 2.80 and 3.10 min [see Fig. 1(a)]. The mass spectra of these eluent fractions, shown in Fig. 2, confirmed the presence of trimethylbenzene in both isomeric forms: the main GC peak (at 2.80 min) corresponded to 1,2,4-TMB, while the smaller peak (at 3.10 min) corresponded to either 1,3,5-TMB or 1,2,3-TMB, which existed as impurities in the solvent. The major ions in the mass spectra were seen at 120, 105, 91, and 77 Da and were consistent with those expected from trimethylbenzene. In contrast, no TMB molecules could be extracted from the aged solid, as confirmed by the absence of the corresponding GC peaks from the spectrum [see Fig. 1(b)]. These data support the observation of partial solubility behavior of the as-made solid, suggesting a possible partial polymerization in the sample, which appears to arise from the slow growth of the nanowires. The data also suggest a likely full polymerization in the aged solid, wherein all the TMB molecules appear to have chemically bonded to C_{60}, resulting in an extensive, nonsoluble polymeric network.

B. ^{13}C-NMR spectroscopic measurement and the polymerization bonding mode

In order to confirm the polymerization and elucidate the nature of the bonding mode involved, we performed ^{13}C NMR spectroscopic studies on both as-made and aged specimens, and on raw C_{60} powder (99.9%, SERS Ltd.) as well as 1,2,4-TMB solvent (98%, Aldrich) (see Fig. 3). Some assignments are immediately suggested by a comparison with the spectra of the pure precursor materials, namely, the pristine C_{60} [see Fig. 3(a)] and pure 1,2,4-TMB [see Fig. 3(b)]. The broad peak at 22.5 ppm in the as-prepared C_{60} TMB adduct [see Fig. 3(c)] results from the three methyl groups of 1,2,4-TMB (19.8, 20.2, and 21.5 ppm), the signal at 129.9 ppm in the same spectrum to benzyl carbons of the adducted 1,2,4-TMB (cf. signals at 127.0, 130.2, and 131.1 ppm in liquid 1,2,4-TMB), that at 135.2 ppm to the quaternary benzyl carbons (cf. signals at 133.9, 135.7, and 136.8 ppm in liquid 1,2,4-TMB), and that at 143.3 ppm to the C_{60} component of the adduct (cf. signal at the same chemical shift in pure C_{60}). Apart from these, it is crucial to note the new peak exhibiting a chemical shift of 30.4 ppm in the spectrum. This is consistent with the presence of methylene carbon atoms directly bonded to aromatic rings,[61] providing direct evidence for polymerization.

A comparison of the ^{13}C-NMR spectra of the as-prepared and the aged [see Fig. 3(d)] materials clearly indicates that, although signals in each sample are consistent with one another, in the latter case the peaks are much broader. This is

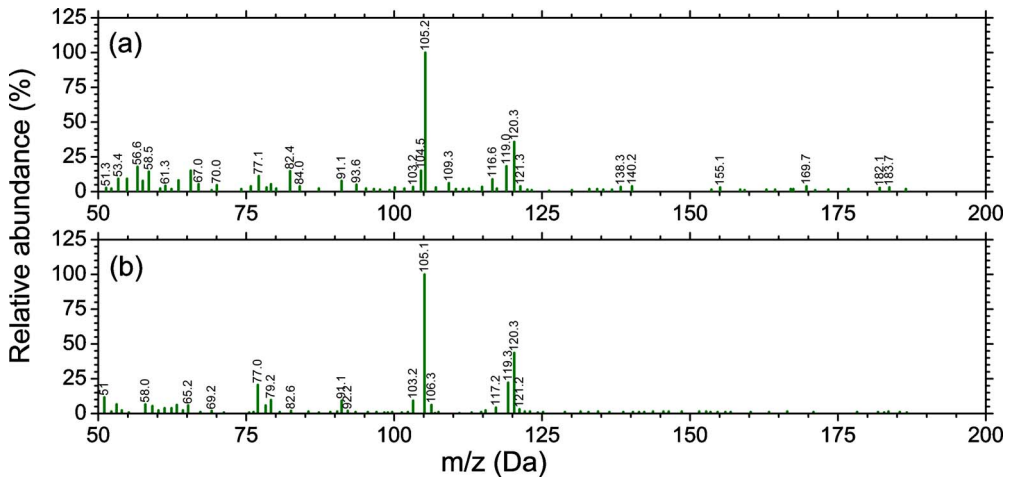

FIG. 2. (Color online) MS analysis of C_{60}TMB nanowires. The profiles (a) and (b) correspond to the GC peaks at 2.80 and 3.10 min (elution times) as shown in Fig. 1(a).

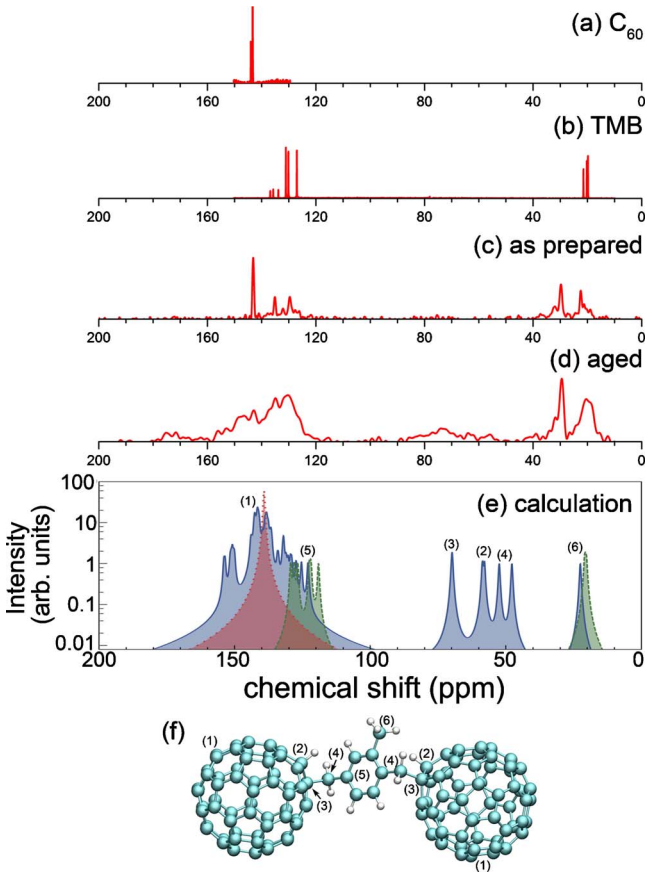

FIG. 3. (Color online) (a) Direct polarization MAS ^{13}C solid state spectrum of pure C_{60}. (b) Solution-state (in deuterochloroform) ^{13}C NMR spectrum of pure 1,2,4-trimethylbenzene. (c) Solid-state CP-MAS ^{13}C NMR spectrum of the as-prepared C_{60}-1,2,4-trimethylbenzene adduct. (d) Solid-state CP-MAS ^{13}C NMR spectrum of the aged C_{60}-1,2,4-trimethylbenzene adduct. (e) The spectra calculated using the *ab initio* B3LYP/6-31G(d) method. Solid line (blue fill (in the online version)), dashed line (green fill (in the online version)), and dotted line (red fill (in the online version)) show the corresponding spectra for the C_{60}-TMB-C_{60} complex as shown in (f), pure 1,2,4-trimethylbenzene and pristine C_{60}, respectively. The numbers labeled in (e) show the chemical shifts of the corresponding carbon atoms marked in (f).

consistent with the structural diversity and heterogeneity expected in the aged sample. In addition, a characteristic fingerprint of the spectrum of the aged nanowires is the emergence of three broad peaks at ~56, ~64, and ~73 ppm. These signals are consistent with sp^3 carbon atoms reported in the literature for polymeric C_{60},[31,62,63] and they provide direct evidence for the formation of covalent bonds between molecules. They are consistent with what would be expected of the three sp^3 carbons marked (2), (3), and (4) in Figs. 3(e) and 3(f). These three carbon atoms are generated as a result of polymerization, as indicated by our theoretical analysis (see below) and their spectroscopic observation serves to provide further evidence of polymerization in addition to our observation of the methylene carbon centers present in the polymeric network.

The ^{13}C-NMR spectroscopic data also indicate the plausibility of polymerization proceeding via conversion of the methyl carbons of TMB into methylenes when reacting with C_{60} units to yield covalent C-C_{60} bonds. Such a reaction logically leads to the formation of a polymethylated aromatic chain structure, i.e., a (-C_{60}TMB-)$_n$ type of copolymer. As such, the chemical shift of the methylene carbons in the polymeric structure, as observed at δ=30.4 ppm, is totally comparable to that of a structurally closely related multisubstituted diphenylmethane such as 2, 4, 6, 2′, 4′, 6′-hexamethyl diphenylmethane (δ=31.2 ppm).[61,64,65] A detailed comparison of the chemical shifts of the structurally related molecules, based on both experimental measurements and theoretical calculations, is presented in Table I.

A comparison of the ^{13}C-NMR data with that obtained by GC-MS reveals that polymerization occurred following the nanowire growth but that the reaction was not fully completed when the nanowire growth ceased. Thus, significant quantities of isolated TMB molecules remained unreacted in the crystalline lattice. These molecules could be easily extracted by dissolution of the crystal in a suitable organic solvent, as indicated by the GC-MS data. Evidently, polymerization continued in the nanowires until all TMB molecules were covalently bonded to adjacent fullerenes, at which point the extraction of further TMB molecules became impossible. On the basis of these analyses, a schematic illustrating the polymeric structure is shown in Fig. 4.

C. Spectroscopic characterization by laser-Raman, SEM, HRTEM, and SAED

Our observations suggest that the polymerization results from a process whereby nanowires undergo a chemical transformation in the crystalline lattice. The fixed lattice positions of the fullerene molecules render it straightforward for the guest TMB species to form bonds with them. Micro-Raman spectroscopic characterization (Ar^+ ion excitation laser, λ =514 nm, spot size ~10 μm) shows that, with the exception of the high-frequency and strongest Ag-symmetry "pentagonal-pinch" (pp) mode at ~1468 cm^{-1}, the other Raman-active modes cannot be clearly identified in the polymerized sample (see Fig. 5, upper line). This contrasts with the spectrum of the as-prepared solid (see Fig. 5, lower line) and suggests that polymerization has significantly reduced the freedom with which the carbons in C_{60} vibrate. Consistent with ^{13}C NMR spectroscopic data, the lack of redshift of the pp mode to ~1458 cm^{-1} clearly indicates that the polymer does not adopt the [2+2] cycloadduction mode as reported for pure C_{60} thin films.[23] Moreover, SEM, HRTEM, and SAED studies on the polymerized nanowires (see Fig. 6) indicate that the (-C_{60}TMB-)$_n$ nanopolymers have retained both the crystal morphology and structure of their parent nanowires,[37,38] reinforcing the view that the polymerization is through a solid-state topochemical event.

D. Favorable polymerization pathways

Detailed investigations of the polymerization reaction mechanism and the nature of the associated bonding mode have been undertaken theoretically. Two possible polymer-

TABLE I. ^{13}C NMR spectroscopic data (ppm) of the molecules of C_{60}, 1,2,4-trimethylbenzene, 2, 4, 6, 2′, 4′, 6′-diphenylmethane, and the $(-C_{60}TMB-)_n$ nanopolymer. The values in brackets indicate chemical shifts calculated in this work using the B3LYP/6-31G(d) method. The values in bold numbers are the chemical shifts measured in this work.

Carbon position	Pristine C_{60}	1,2,4-trimethylbenzene (1,2,4-TMB)	2, 4, 6, 2′, 4′, 6′ hexamethyl diphenylmethane	The $(-C_{60}TMB-)_n$ nanopolymer
C (sp^2 in C_{60})	142.7[a]			143.3
	143.3			(130.3–154.0)
	(139.2)			
Ring carbons: C-1		133.4[b,d], 133.9[d], (126.8)	134.6[c]	(129.0)
C-2		136.3[b,d], 136.8[d], (129.4)	136.3[c,d]	135.2[d], (132.0)
C-3		130.5[b], 131.1, (122.5)	129.0[c]	129.9, (127.4)
C-4		135.2[b,d], 135.7[d], (128.1)	134.5[c,d]	(129.5)
C-5		126.7[b], 127.0, (119.1)	129.0[c]	(123.0)
C-6		129.8[b], 130.2, (121.9)	136.3[c,d]	(125.4)
1-CH_3		19.1[b], 19.8, (20.3)		
2-CH_3		19.5[b], 20.2, (20.7)	20.9[c]	
3-CH_3				22.5, (22.6)
4-CH_3		20.9[b], 21.5, (21.0)	20.9[c]	
5-CH_3				
6-CH_3			20.9[c]	
—CH_2—			31.2[c]	30.4, 55.9
C (sp^3 in C_{60})				(28–43, 47.8, 52.4)
				73.2, 63.5
				(69.6, 58.6)

[a]Reference 64.
[b]Reference 65.
[c]Reference 61.
[d]Quaternary carbons on the benzene ring.

ization scenarios have been considered: the first involves two C_{60} molecules and a TMB molecule and utilizes two methylene bridges; the second involves three C_{60} molecules and a TMB and uses all the three possible linkages. The product predicted from the reaction between two C_{60} molecules and one TMB molecule is a molecular complex, $C_{60}XC_{60}$, where X denotes a residue derived from the TMB molecule. There are two possibilities regarding the reaction pathway

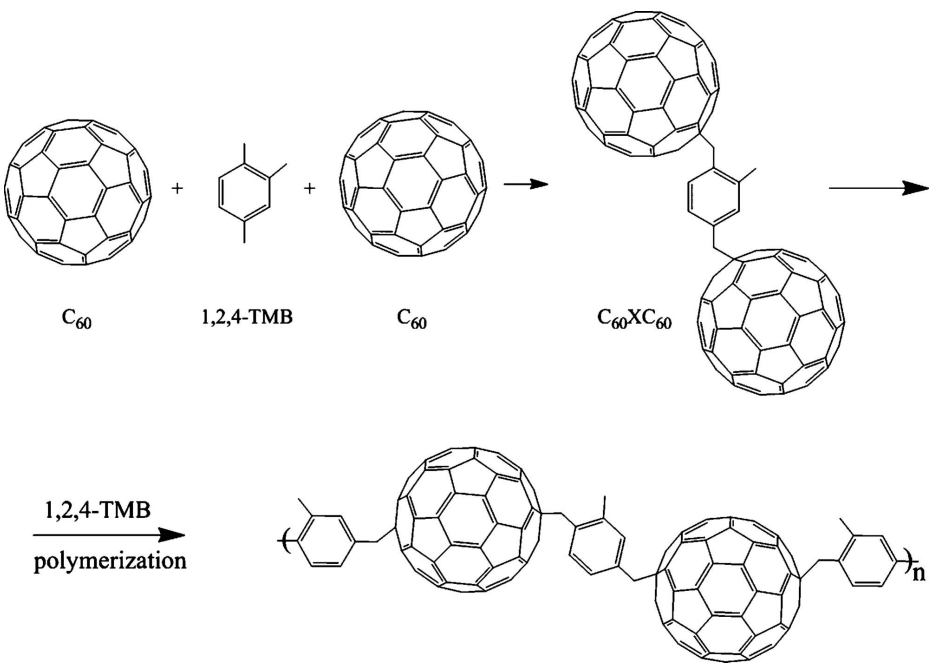

FIG. 4. A schematic shows the polymerization reaction pathway. The label X in the dimer indicates a residue derived from the TMB molecule during the reaction. Hydrogen atoms are omitted in this diagram for clarity.

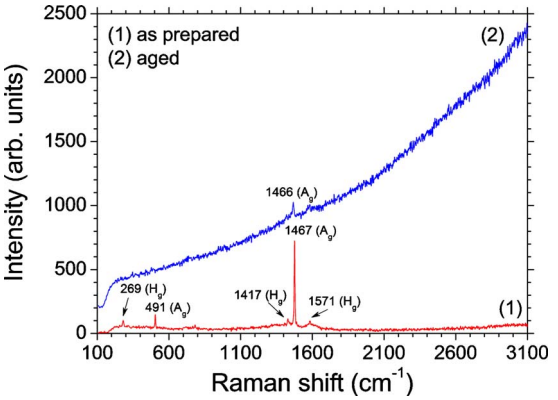

FIG. 5. (Color online) Laser micro-Raman spectroscopic analysis shows the profiles of the as-made (1) and the aged (2) C_{60}TMB nanowire sample.

$$C_{60} + TMB + C_{60} \rightarrow C_{60} - TMB^{-2H} - C_{60} + H_2 + \Delta E_1, \quad (7)$$

$$C_{60} + TMB + C_{60} \rightarrow HC_{60} - TMB^{-2H} - C_{60}H + \Delta E_2, \quad (8)$$

where TMB^{-2H} represents the TMB molecule with two hydrogen atoms removed and ΔE_1 and ΔE_2 are the corresponding reaction enthalpies.

In reaction (7), two C-H bonds in the TMB molecule (likely at the 1- and 4-methyl positions) are broken and two C-C_{60} bonds are formed. As a consequence, an H_2 molecule is released. Reaction (8) occurs in a similar way, but instead of forming a H_2 molecule, the released H-atoms bond to either fullerene. The structures of the computed (by the *ab initio* B3LYP/6-21G method)[54] reaction products, C_{60}-TMB^{-2H}-C_{60} and HC_{60}-TMB^{-2H}-C_{60}H, are shown in Figs. 7(a) and 7(b), respectively, along with their associated distances between the two fullerenes.[54]

To quantify ΔE_1 and ΔE_2, we first optimized the structures of all the reaction partners and calculated their energies using the methods described in Sec. III. The total energies of the molecules involved in the reactions are summarized in Table II. The calculated enthalpies are as follows: ΔE_1 =59.8 kcal mol^{-1} and ΔE_2=−11.7 kcal mol^{-1}. Note that the B3LYP/STO-3G method gives somewhat different values for the reaction enthalpies. This method is less accurate than the B3LYP/6-21G method, and can, therefore, be only used for a qualitative analysis of the system.[54]

The fact that reaction (7) is endothermic can be understood in terms of the changes in electron configuration for

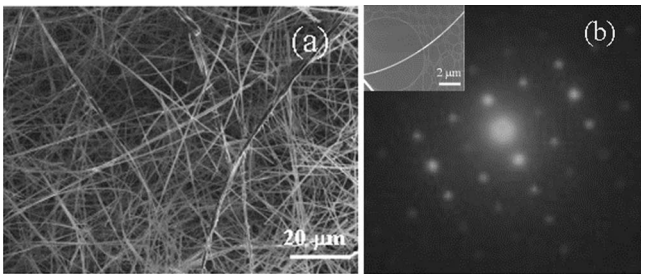

FIG. 6. (a) SEM image of the $(-C_{60}TMB-)_n$ nanopolymer. (b) SAED pattern shows the crystalline nature of the polymer. The inset in (b) is a typical TEM image of a nanopolymer associated with the SAED measurement.

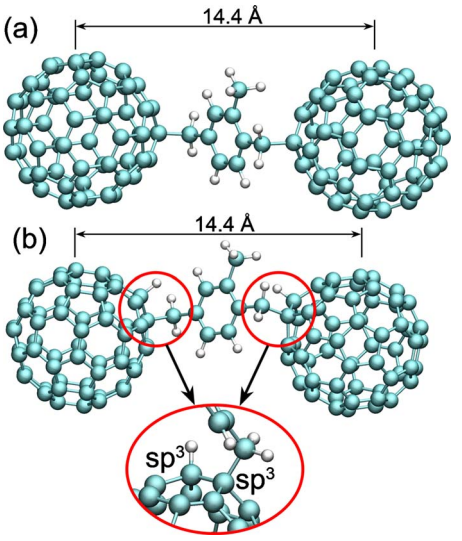

FIG. 7. (Color online) Computed structures of the reaction products (a) C_{60}-TMB^{-2H}-C_{60} and (b) HC_{60}-TMB^{-2H}-C_{60}H, corresponding to reactions (7) and (8) in the text. The distances between the fullerenes are indicated and they are the values calculated using the B3LYP/6-21G method. The inset shows the sp^3 hybridization of the fullerene carbon atoms resulting from the formation of the covalent bonds with TMB^{-2H}.

TABLE II. Total energies of the molecules involved in the analyzed polymerization reactions and the enthalpies (ΔE) of reactions (7)–(9) calculated using *ab initio* B3LYP/6-21G and B3LYP/STO-3G methods. The energies are given in atomic units. The superscripts (a) and (b) indicate the isomers shown in Fig. 9. The enthalpies in brackets correspond to the values calculated using the B3LYP/STO-3G method while the values without brackets were calculated using the B3LYP/6-21G method. (1 a.u.=27.2116 eV =627.499 kcal mol^{-1}).

Molecules	Total energy B3LYP/6-21G (a.u.)	Total energy B3LYP/STO-3G (a.u.)	ΔE (kcal mol^{-1})
1,2,4-TMB	−349.8621	−345.9655	
C_{60}	−2283.9917	−2258.2208	
H_2	−1.1706	−1.1655	
C_{60}-TMB^{-2H}—C_{60}	−4916.5795	−4862.4656	+59.8
			(+51.0)
HC_{60}-TMB^{-2H}—C_{60}H	−4917.8642	−4861.1603	−11.7
			(−36.71)
$3C_{60}TMB^{(a)}$		−7120.7144	
			(−53.6)
$3C_{60}TMB^{(b)}$		−7120.7144	
			(−55.1)

carbon atoms in C_{60} following the reaction. Every carbon atom in a fullerene has three covalent bonds with its neighbors, two of which are single, and one of which is double. The carbon atoms in a fullerene therefore exhibit sp^2 hybridization, but the framework is slightly distorted because of the surface curvature. To attach a TMB molecule to a fullerene, it is necessary to break a double bond in the carbon shell, leading to the formation of two unsaturated carbon atoms. In reaction (7) the TMB^{-2H} complex caps one of these carbon atoms in each fullerene, rendering the carbon sp^3 hybridized but leaving the neighboring carbon unsaturated—an energetically unfavorable scenario. In contrast, reaction (8) is exothermic because the hydrogen atoms released from the TMB molecule cap the neighboring unsaturated carbon atoms in each of the C_{60} fragments. Thus, both carbon atoms that have undergone reaction in either fullerene have become sp^3 hybridized [as illustrated by the inset of Fig. 7(b)]. It is noted that the C_{60}-TMB^{-2H}-C_{60} complex can then undergo subsequent reactions, in which two fullerene cages continue to react with a TMB to form a polymeric network as shown in Fig. 4.

This result is consistent with our elemental analysis for a polymerized sample where parallel analyses yield an average hydrogen content of 1.35 wt %, consistent with the molar ratio of ~1:1 for 1,2,4-TMB over C_{60} in the solid, as measured previously by thermal gravimetric analysis.[37] Reaction (8) has some similarities to the Prato and Bingel reactions widely known in fullerene chemistry.[66] In these reactions an organic molecule reacts with a double bond in C_{60} and forms a ring peripheral to the fullerene superstructure. The calculated reaction enthalpy suggests that reaction (8) is energetically favorable and therefore is likely to occur.

To understand the mechanism by which reaction (8) occurs we have calculated the enthalpy of this process as a function of the separation between the 1,2,4-TMB and fullerenes (see Fig. 8). Although the energy landscape of reaction (8) is not important for the conclusions drawn in this paper, it provides a more detailed understanding of the polymerization process. The reaction coordinate, separating the adducts $2C_{60}$+TMB and the product HC_{60}-TMB^{-2H}-$C_{60}H$ of reaction (8) is defined nontrivially because of the complexity of reaction (8). Therefore, in Fig. 8 we plot the reaction coordinate in arbitrary units.

Figure 8 shows the results of a constrained calculation performed by using the semiempirical AM1 method. By constraining one degree of freedom in the HC_{60}-TMB^{-2H}-$C_{60}H$ complex we performed optimization of the system in respect to all other degrees of freedom and calculated the energy of the corresponding stable configuration. By sequential constraining of different degrees of freedom we have computed the transformation of the bonded HC_{60}-TMB^{-2H}-$C_{60}H$ complex into the unbonded $2C_{60}$+TMB state.

Reaction (8) passes through three intermediate stages. Starting from the initial HC_{60}-TMB^{-2H}-$C_{60}H$ structure (see state 1 in Fig. 8) the two fullerenes sequentially rotate around the C—C bond that connects them to the TMB^{-2H} bridge. In the course of this rearrangement, the hydrogen atoms $H^{(1)}$ and $H^{(2)}$, bonded to the corresponding fullerenes $C_{60}^{(1)}$ and $C_{60}^{(2)}$, become oriented toward the -CH_2- units of the TMB^{-2H} bridge. The rearrangement occurs sequentially, involving

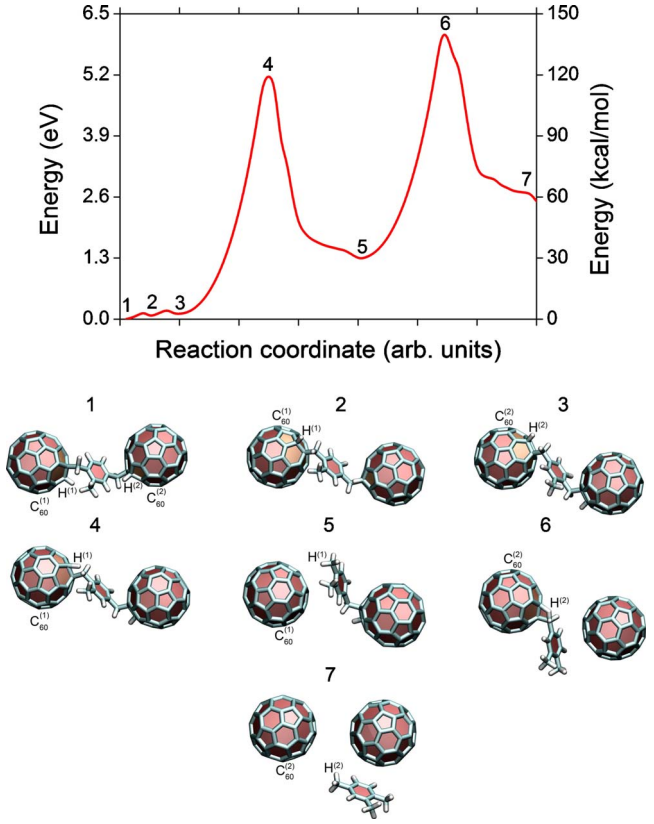

FIG. 8. (Color online) Enthalpy of reaction (8) calculated using the semiempirical AM1 method (Refs. 55 and 56) plotted as a function of the reaction coordinate, which characterizes the separation of the 1,2,4-TMB molecule from the fullerenes in the HC_{60}-TMB^{-2H}-$C_{60}H$ complex (see text). The indices in the plot mark the different stages of the reaction that are illustrated in the lower part of the figure.

first $C_{60}^{(1)}$ and then $C_{60}^{(2)}$, and leads to the formation of two stable states of the HC_{60}-TMB^{-2H}-$C_{60}H$ complex, denoted as 2 and 3 (see Fig. 8). The energies of stable configurations are 0.058 eV=1.34 kcal/mol and 0.111 eV=2.56 kcal/mol, respectively (relative to the energy of ground state 1). The respective transition barriers are $\Delta E_{1\to 2}$=0.151 eV =3.48 kcal/mol and $\Delta E_{2\to 3}$=0.141 eV=3.25 kcal/mol. The energies involved in this rearrangement are relatively low because it involves the transformation around the C—C bond, within which both carbon atoms are sp^3 hybridized, i.e., relatively easy rotation is allowed.

In the second stage of reaction (8) hydrogen atom $H^{(1)}$ from $C_{60}^{(1)}$ moves toward the methyl side chain of TMB^{-2H}. This results in a rapid increase in system energy until a transition state is formed (see state 4 in Fig. 8). The energy of this transition state is 5.113 eV=117.91 kcal/mol higher than the energy of state 3. Note that in this state the hydrogen atom is still weakly bound to $C_{60}^{(1)}$. Next, a critical rearrangement occurs in the system: the hydrogen atom $H^{(1)}$ transfers to the TMB^{-2H} bridge, which in turn becomes detached from $C_{60}^{(1)}$. As a result, the sp^3-hybridized carbon atoms in $C_{60}^{(1)}$ become sp^2-hybridized (see state 5 in Fig. 8). The energy of the intermediate C_{60}+TMB^{-H}-$C_{60}H$ formed at this stage of reaction (8) is 1.283 eV=29.59 kcal/mol higher than the energy of the initial state 1.

The last stage of reaction (8) involves $C_{60}^{(2)}$ and is similar to the second stage of the reaction: first, transition state is formed (state 6 in Fig. 8), which is then transformed to the final state (state 7) of the reaction, in which the TMB molecule is detached from both fullerenes. The energy of the final product is 2.508 eV=57.84 kcal/mol higher than the energy of the initial state (state 1). Figure 8 shows that the barriers associated with fullerene detachment from TMB^{-2H} or TMB^{-H} are asymmetric, i.e., $\Delta E_{3\rightarrow 5}=5.113$ eV $=117.91$ kcal/mol and $E_{5\rightarrow 7}=4.806$ eV=110.83 kcal/mol while $E_{5\rightarrow 3}=3.941$ eV=90.88 kcal/mol and $E_{7\rightarrow 5}=3.581$ eV=82.58 kcal/mol.

The energies calculated using the semiempirical AM1 method differ significantly from the values calculated using the *ab initio* B3LYP/6-21G method. Thus, the energy difference between the starting compounds and the final products of reaction (8) calculated with B3LYP/6-21G is −11.7 kcal/mol (see Table II) while by AM1 it is −57.84 kcal/mol (see Fig. 8). This large discrepancy arises because of significant simplifications made in the AM1 method. Although the AM1 method is not very precise in energy calculations, it likely correctly reproduces the energies within an order of magnitude and makes it possible to describe the geometry of the system reasonably well. The major advantage of the AM1 method lies in its computational speed. Indeed, to perform one optimization step of the HC_{60}-TMB^{-2H}-$C_{60}H$ complex one needs ~20 s using the AM1 method and ~6.25 h using the B3LYP/6-21G method (the timings correspond to a standard personal computer with an Intel Core 2 Duo processor and 6 GB RAM). To calculate the energy profile shown in Fig. 8, one needs to perform about 1000 constrained optimization calculations. These can be achieved in ~5.5 h with the AM1 method and ~260 days using the B3LYP/6-21G method. Moreover, the results shown in Fig. 8 correspond to the best reaction path found connecting the two states of reaction (8). To describe this transformation many trial calculations involving different degrees of freedom in the system were made in order to find the lowest transition barriers. The results shown in Fig. 8 correspond to the lowest barrier energies found by the calculation. Such a computation is hardly possible with the computer time demanding B3LYP method.

A second and more complex polymerization pathway that can be envisaged involves three fullerenes and one TMB. By analogy to Eq. (2), the reaction can be written as

$$C_{60} + TMB + C_{60} + C_{60} \rightarrow 3C_{60}TMB + \Delta E_3. \qquad (9)$$

The possible geometrical arrangements of two low-energy isomers of $3C_{60}TMB$ (B3LYP/STO-3G method) are shown in Fig. 9. These structures are constructed in a similar way to the $2C_{60}TMB$ complex but in this case three C-H bonds have been broken in the TMB unit and the resulting $3C_{60}TMB$ complex adopts a triangular configuration. The total energies calculated for two optimized isomeric structures of the $3C_{60}TMB$ are shown in Table II, corresponding to the two complexes shown in Fig. 9. The calculated enthalpies are $\Delta E_3=-53.64$ kcal mol^{-1} and $\Delta E_3=-55.11$ kcal mol^{-1}, for the product isomers (a) and (b), respectively. In either case, it is clear that reaction (9) is exothermic and thus energetically favorable.

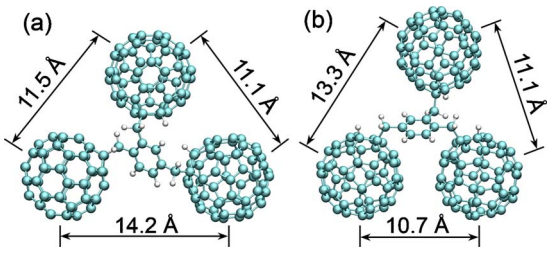

FIG. 9. (Color online) Calculated structures of two low-energy isomers of the $3C_{60}TMB$ complex as the product of reaction (9) in the text. The distances between fullerene centers correspond to the geometries optimized at the B3LYP/STO-3G level of calculation.

E. Structural calculations and analysis

In order to understand how the 1,2,4-TMB molecules bond to fullerene motives in the nanowires, we have studied the geometrical constraints of the unit cell of the crystal lattice. As follows from the SEM and SAED measurements performed on the aged nanowires (discussed in Sec. IV C), the polymerized nanowires largely preserve the crystalline structure of the as-grown nanowires discussed in Ref. 37). Therefore, a polymerization process is only possible if the distances in the nanowire unit cell are such that the TMB molecule can form covalent bonds with the fullerenes without significantly disturbing the unit-cell structure. In this section we analyze the geometrical constraints in the nanowire and, from this analysis, establish the possible polymerization modes in the nanowires. Figure 10(a) shows the geometry of the nanowire unit cell and its dimensions, based on the experimental data.[37,38,67] For simplicity, here we do not show the embedded TMB molecules. As discussed before, a TMB molecule may link two fullerenes together, and if this mode is repeated periodically, the crystalline nanowire would turn into a nanopolymer.

In Fig. 10(b) we show a C_{60}-TMB-C_{60} complex, where two fullerenes are covalently linked by a 1,2,4-TMB molecule. In this case the distance between the two fullerenes is 14.4 Å, very close to one of the interfullerene spacings measured for the unit cell [14.5 Å, Fig. 10(a)]. The linkage is thus highly likely to occur in the unit cell and the C_{60}-TMB-C_{60} complex is likely to be a possible building block for the polymerization. Figures 10(c) and 10(d) illustrate two possible linking schemes between the fullerenes, where the bars between fullerenes represent TMB molecules. Based on the preferential crystal-growth directions studied previously,[37,38] this polymerization may occur along either the *a* [see Fig. 10(c)] or the *b* axis [see Fig. 10(d)], with the linkages corresponding to the two schemes as shown in the figures.

It is important to stress that a C_{60}-TMB-C_{60} complex has several stable isomeric configurations with different C_{60}-C_{60} distances. To illustrate this fact, in Fig. 11 we show how the the distance between two fullerenes in a C_{60}-TMB-C_{60} complex depends on an angle φ, which is de-

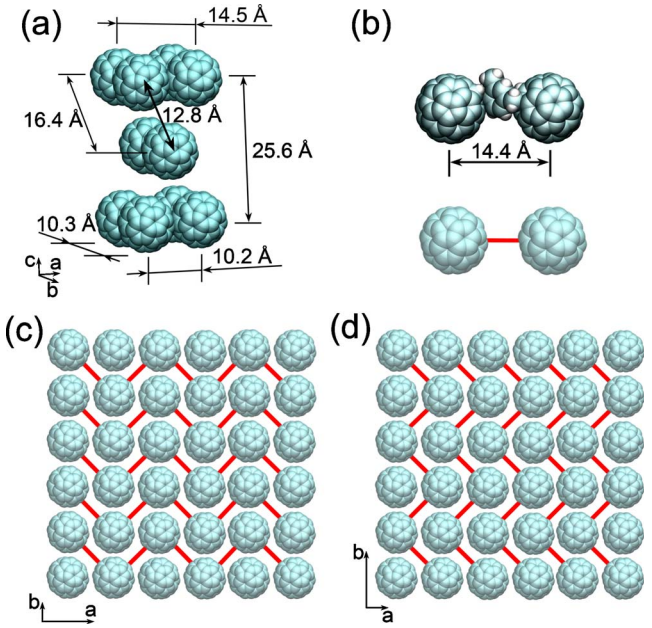

FIG. 10. (Color online) Possible polymerization scenarios of the C_{60}TMB 1D nanocrystals. In (a) we show the geometry of the unit cell (the TMB molecules embedded in the unit cell are not shown). The distances between the centers of the fullerenes are indicated. The geometry of a C_{60}-TMB-C_{60} molecule is shown in (b). The distance between the two fullerenes in this case is 14.4 Å, very close to the dimensions of the unit cell. Plots (c) and (d) demonstrate the cross section of a nanowire, viewed along the *c* axis, and illustrate two possible linking schemes between the fullerenes. The bars between the fullerenes indicate the TMB molecules. The polymerization can occur along either the *a* (plot c) or the *b* axis (plot d) of a nanowire (Refs. 37 and 38).

fined as the separation degree between the planes formed by atoms (1)-(2)-(3) and atoms (2)-(3)-(4), as shown in the figure. As the bonds connecting two C_{60} units and a TMB^{-2H} are not collinear, the center-to-center distance changes upon

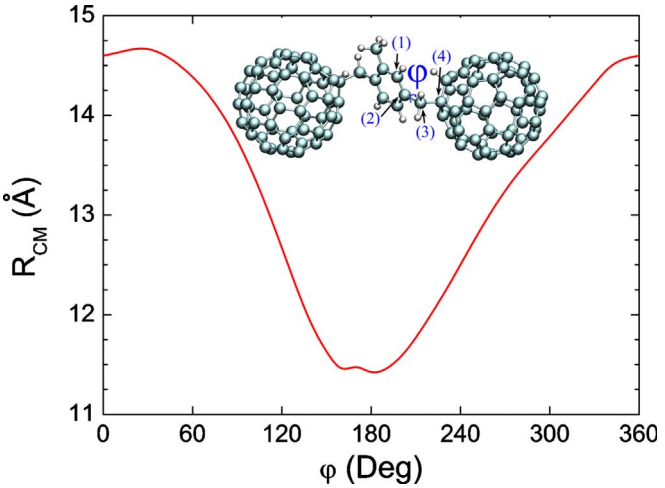

FIG. 11. (Color online) Distance between the centers of two fullerenes in a C_{60}-TMB-C_{60} complex as a function of angle φ, which is defined as the angle between the planes formed by the atoms (1)-(2)-(3) and (2)-(3)-(4), as shown in the inset.

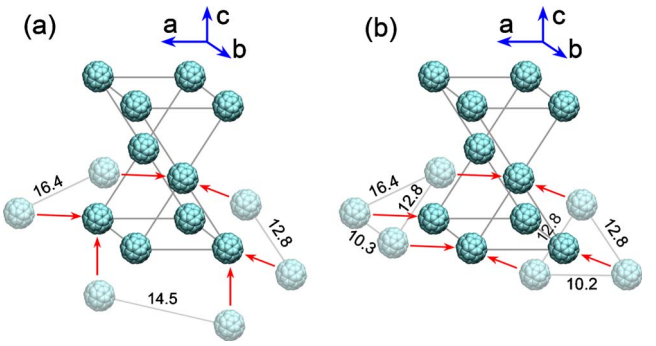

FIG. 12. (Color online) Possible fitting sites of (a) the $2C_{60}$TMB complex and (b) the $3C_{60}$TMB complex, in the unit cell of the parent nanowire. Distances are given in Ångstroms and correspond to experimental data (Ref. 37).

rotation of the fullerenes. As can be seen from Fig. 11, such a distance varies from 11.5 to 14.5 Å, and match the distances between fullerenes in the unit cell [as indicated in Fig. 10(a)].

Based on this geometrical analysis, we have noted that there appear to be three possibilities for fusing a TMB^{-2H} molecule in between two fullerenes in the unit cell, as illustrated by the three sets of C_{60} dimers marked in Fig. 12(a). Except these possibilities, the distances between any other two fullerenes are either too small or too large and are thus incompatible with the requirement for a topochemical polymerization to occur. Note that although the distance 16.4 Å in the unit cell is somewhat larger than the distances shown in Fig. 11, the related fusion mode is still possible because the distance between fullerenes in a C_{60}-TMB-C_{60} complex may further change under certain conditions. Some deviations are expected because the C_{60}-TMB-C_{60} complex was optimized *in vacuo* without accounting for other related constituents in the polymer. Also, the complex has many isomers because in the crystal unit cell a fullerene has many different atomic sites to which a TMB^{-2H} molecule may attach.

Similarly, Fig. 12(b) shows two possible fitting sites for a $3C_{60}$TMB complex in the unit cell. This structural analysis clearly demonstrates that a 1,2,4-TMB molecule can easily stitch two fullerenes together within a nanowire without disturbing the lattice structure. This conclusion is in excellent agreement with the experimental studies with SEM, HR-TEM, and SAED, as described earlier.

F. Theoretical analysis of the ^{13}C-NMR spectra

Our experimentally measured chemical shifts are supported by the calculated values as shown by Fig. 3(e). To do the calculation, we have applied the *ab initio* B3LYP/6-31G(d) method to pristine C_{60} (dotted line, red fill (in the online version)), pure 1,2,4-TMB (dashed line, green fill), and the C_{60}-TMB-C_{60} complex (solid line, blue fill). Since many of the calculated chemical shifts are degenerate, Lorentzian broadening for each line is assumed

$$F(\delta) = \frac{1}{\pi}\sum_{i=1}^{N} \frac{1/2^{\sigma}}{(\delta - \delta_i)^2 + (1/2^{\sigma})^2}. \tag{10}$$

Here δ_i is the calculated chemical shift and $\sigma = 2/\pi$ is the width of peaks at half maximum intensity. The calculated

^{13}C-NMR spectra are plotted on a logarithmic scale for better visualization.

The calculated chemical shifts for pure C_{60} and 1,2,4-TMB are in good agreement with experiment. The observed signal for C_{60} at 143.3 ppm is only 4 ppm higher than the calculated, and the calculated shift for the ring carbons of TMB is only 7–8 ppm lower than the observed. Also, the calculated values for the methyl groups perfectly reproduce the measured data (within an error of less than 1.0 ppm). These comparisons enable us to conclude that the accuracy of the calculation is on the order of ~5–8 ppm, which is sufficient for an unambiguous characterization of the calculated NMR peaks in this work.

In the previous section we suggested that the C_{60}-TMB-C_{60} complex was a building block in the polymerization. The calculated ^{13}C-NMR spectrum for the complex strongly supports this view by virtue of its excellent agreement with the experimental result. Crucially, the emergence of four peaks in the range of 45–80 ppm, consistent with the observed set of broad peaks at 55–85 ppm, corresponds to the chemical shifts of the carbon atoms (2), (3), and (4), respectively, as marked in Fig. 3(f). These three atoms participate in the bonds formed between C_{60} and 1,2,4-TMB molecules in the polymerized network.

The observed peak at 30.4 ppm can be interpreted as the response from methylene carbons cross-linking adjacent 1,2,4-TMB molecules due to polymerization. This view is strongly supported by literature report of the structurally closely related framework of multisubstituted diphenylmethane (see Table I).[61,64,65] Within the accuracy of the calculation, it is also consistent with our calculations for TMB-TMB dimers, which predict the corresponding chemical shift to be in the range of 28–43 ppm, depending on the bonding mode adopted by the dimers and the relative orientations of the adjacent TMB molecules involved (see Fig. 13). Figure 13(a) shows an example of a dimer in which the two benzene rings are perpendicular to each other and the two TMB molecules are bonded together through two methylene carbons corresponding to the ring positions of 1- and 4-methyl, respectively. In this case, the two methylenes yield two closely placed peaks at 35.7 ± 7 and 37.8 ± 7 ppm. Figure 13(b) shows another example of a dimer in which the two TMB molecules are linked by only one methylene carbon which exhibits a chemical shift of 38.4 ppm. Figure 13(c) shows the third example of such a dimer isomer, where the two TMB molecules are linked by two identical methylene carbons but the two benzene rings are parallel to each other. In this case the chemical shift calculated is 43.4 ppm. These analyses suggest that the chemical shift of the methylene carbons is sensitive to the surrounding atoms, and that the peak observed at 30.4 ppm hint at some specific bonding mode and/or relative orientations between TMB molecules in the polymeric chains. Moreover, the enthalpy calculated for such a dimerization reaction using the B3LYP/6-21G method is −19.2 kcal/mol, indicating that the dimerization reaction for polymerization is energetically favorable.

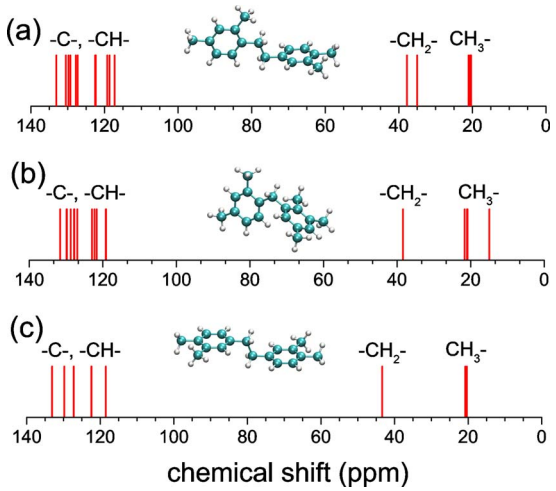

FIG. 13. (Color online) ^{13}C-NMR spectra calculated for three isomeric states of the TMB-TMB dimer using the *ab initio* B3LYP/6-31G(d) method. The geometries of the molecules used in the calculation are shown in the inset. Labels indicate the chemical shifts of different types of carbon atoms in the system. Note that the chemical shifts in (c) are much more degenerate than (a) and (b) due to the enhanced symmetry of the studied isomer.

V. CONCLUSION AND PERSPECTIVE

We have demonstrated an approach to the preparation of a C_{60}-based polymer nanowire and have established the chemical bonding mode involved in the polymeric chains based on both experimental measurements and theoretical calculations. Importantly, the material adopts a crystalline 1D nanostructure which resembles carbon nanotubes in shape and other important conjugated polymers in structure. Since the material does not contain any metal but is composed almost entirely of carbon (the hydrogen content is only 1.4 wt %), it suggests biological compatibility and it is, perhaps, even more attractive than carbon nanotubes for bioapplications. In addition, the material has further important potential for applications in photoelectrical devices because of the intrinsically large magnitude of the nonlinear optical response of C_{60} and the excellence of its photoinduced charge-transfer properties. Considering all these points, we believe that this work represents a step toward true applications of C_{60} in nanotechnology through the processing of commercially available raw C_{60} powder into a one-dimensional, crystalline, covalently bonded fullerene nanopolymer.

We consider that applications of the reported nanopolymer may be facilitated by a wet chemical approach through surface modification of the material using the rich chemistry of fullerene that has been developed over the last 20 years. Since the nanopolymer is insoluble in common solvents, such surface modification or functionalization should be possible to achieve in either an aqueous or an organic solution without destroying its solid-state structure. Such a wet approach would benefit from low processing cost, the need for only simple apparatus and the possibility of scaling-up to the industrial level. Moreover, the nanopolymer itself not only provides an example of phase transition of the parent nanowire driven by forming and breaking covalent bonds but also illustrates the enduring significance of the original fullerene concept and its versatility as applied to new fullerene-related nanostructures. Finally, the host (C_{60}) and guest (1,2,4-TMB) nature of the polymerization suggests a general host-guest

route to the synthesis of new types of fullerene-based nanopolymers composed of different organic monomers and fullerenes.

ACKNOWLEDGMENTS

We thank support from the European Commission (Project No. NOE EXCELL NMP3-CT-2005-515703). The assistance of Wuzong Zhou, School of Chemistry, St. Andrews University, for carrying out TEM analysis is acknowledged. Computer simulations were carried out at the Frankfurt Center for Scientific Computing.

*jg201@cam.ac.uk
†ilia@fias.uni-frankfurt.de

[1] R. Baughman, A. Zakhidov, and W. de Heer, Science **297**, 787 (2002).
[2] I. A. Solov'yov, M. Mathew, A. V. Solov'yov, and W. Greiner, Phys. Rev. E **78**, 051601 (2008).
[3] Y. Akai and S. Saito, Physica E **29**, 555 (2005).
[4] K. Miyazawa, J. Minato, T. Yoshii, M. Fujino, and T. Suga, J. Mater. Res. **20**, 688 (2005).
[5] L. Wang *et al.*, Adv. Mater. **18**, 1883 (2006).
[6] K. Miyazawa, Y. Kuwasaki, K. Hamamoto, S. Nagata, A. Obayashi, and M. Kuwabara, Surf. Interface Anal. **35**, 117 (2003).
[7] H. Liu *et al.*, J. Am. Chem. Soc. **124**, 13370 (2002).
[8] M. Dresselhaus, G. Dresselhaus, and P. Eklund, *Science of Fullerenes and Carbon Nanotubes* (Academic Press, San Diego, 1996).
[9] C. Lieber and M. Wang, MRS Bull. **32**, 99 (2007).
[10] J. Geng, I. Kinloch, C. Sing, V. Golovko, B. Johnson, M. Shaffer, Y. Li, and A. Windle, J. Phys. Chem. B **109**, 16665 (2005).
[11] O. Stoilova, C. Jerome, C. Detrembleur, A. Mouithys-Mickalad, N. Manolova, I. Rashkov, and R. Jerome, Polymer **48**, 1835 (2007).
[12] S. Ghosh, A. Sood, and N. Kumar, Science **299**, 1042 (2003).
[13] M. Zheng *et al.*, Science **302**, 1545 (2003).
[14] D. Heller, E. Jeng, T.-K. Yeung, B. Martinez, A. Moll, J. Gastala, and M. Strano, Science **311**, 508 (2006).
[15] W. Guss, J. Feldmann, E. O. Gobel, C. Taliani, H. Mohn, W. Muller, P. Haussler, and H. U. ter Meer, Phys. Rev. Lett. **72**, 2644 (1994).
[16] R. Saito, G. Dresselhaus, and M. S. Dresselhaus, Phys. Rev. B **46**, 9906 (1992).
[17] M. Xu, Y. Pathak, D. Fujita, C. Ringor, and K. Miyazawa, Nanotechnology **19**, 075712 (2008).
[18] Y. Wang, Nature (London) **356**, 585 (1992).
[19] V. Solovyeva, K. Keller, and M. Huth, Thin Solid Films **517**, 6671 (2009).
[20] N. Sariciftci, L. Smilowitz, A. Heeger, and W. Wudl, Science **258**, 1474 (1992).
[21] M. Morana, M. Wegscheider, A. Bonanni, N. Kopidakis, S. Shaheen, M. Scharber, Z. Zhu, D. Waller, R. Gaudiana, and C. Brabec, Adv. Funct. Mater. **18**, 1757 (2008).
[22] R. Service, Science **293**, 1570 (2001).
[23] A. Rao *et al.*, Science **259**, 955 (1993).
[24] P. Eklund, A. Rao, P. Zhou, Y. Wang, and J. Holden, Thin Solid Films **257**, 185 (1995).
[25] S. Pekker, A. Janossy, L. Mihaly, O. Chauvet, M. Carrard, and L. Forro, Science **265**, 1077 (1994).
[26] H. Nagashima, M. Nakaoka, Y. Saito, M. Kato, T. Kawanishi, and K. Itoh, J. Chem. Soc., Chem. Commun. **1992**, 377.
[27] K. Geckeler and A. Hirsch, J. Am. Chem. Soc. **115**, 3850 (1993).
[28] F. Wudl, Acc. Chem. Res. **25**, 157 (1992).
[29] Y. Iwasa *et al.*, Science **264**, 1570 (1994).
[30] M. Núñez-Regueiro, L. Marques, J. L. Hodeau, O. Béthoux, and M. Perroux, Phys. Rev. Lett. **74**, 278 (1995).
[31] A. V. Soldatov, G. Roth, A. Dzyabchenko, D. Johnels, S. Lebedkin, C. Meingast, B. Sundqvist, M. Haluska, and H. Kuzmany, Science **293**, 680 (2001).
[32] R. Céolin, J. Ll. Tamarit, D. O. Lopez, M. Barrio, V. Agafonov, H. Allouchi, F. Moussa, and H. Szwarc, Chem. Phys. Lett. **314**, 21 (1999).
[33] A. Balch, J. Lee, B. Noll, and M. Olmstead, J. Chem. Soc., Chem. Commun. 1993, 56.
[34] H. B. Buergi, R. Restori, D. Schwarzenbach, A. L. Balch, J. W. Lee, B. C. Noll, and M. M. Olmstead, Chem. Mater. **6**, 1325 (1994).
[35] K. Miyazawa, C. Nishimura, M. Fujino, T. Suga, and T. Yoshii, Trans. Mater. Res. Soc. Jpn. **29**, 1965 (2004).
[36] K. Miyazawa and K. Hamamoto, J. Mater. Res. **17**, 2205 (2002).
[37] J. Geng, W. Zhou, P. Skelton, W. Yue, I. Kinloch, A. Windle, and B. Johnson, J. Am. Chem. Soc. **130**, 2527 (2008).
[38] J. Geng, I. Solov'yov, W. Zhou, A. Solov'yov, and B. Johnson, J. Phys. Chem. C **113**, 6390 (2009).
[39] I. Solov'yov, J. Geng, A. Solov'yov, and B. Johnson, AIP Conf. Proc. 1197, 89 (2009).
[40] M. J. Frisch *et al.*, GAUSSIAN 03, Revision C.02 (Gaussian, Inc., Wallingford CT, 2004).
[41] A. Lyalin, I. A. Solov'yov, A. V. Solov'yov, and W. Greiner, Phys. Rev. A **75**, 053201 (2007).
[42] I. A. Solov'yov, A. V. Solov'yov, and W. Greiner, Phys. Rev. A **65**, 053203 (2002).
[43] A. Lyalin, I. A. Solov'yov, A. V. Solov'yov, and W. Greiner, Phys. Rev. A **67**, 063203 (2003).
[44] I. Solov'yov, A. Yakubovich, A. Solov'yov, and W. Greiner, J. Exp. Theor. Phys. **102**, 314 (2006).
[45] A. Yakubovich, I. Solov'yov, A. Solov'yov, and W. Greiner, Eur. Phys. J. D **39**, 23 (2006).
[46] I. A. Solov'yov, A. V. Yakubovich, A. V. Solov'yov, and W. Greiner, Phys. Rev. E **73**, 021916 (2006).
[47] *Atomic Clusters and Nanoparticles*, Les Houches Session LXXIII, edited by C. Guet, P. Hobza, F. Spiegelman, and F. David (EDP Sciences and Springer-Verlag, Berlin, 2001).
[48] *Latest Advances in Atomic Cluster Collisions Fission, Fusion, Electron, Ion and Photon Impact*, edited by A. Solov'yov and J.-P. Connerade (World Scientific Press, Singapore, 2004).
[49] L. Lindgren and J. Morrison, *Atomic Many-Body Theory* (Springer-Verlag, New York, Berlin, 1986).
[50] P. Hohenberg and W. Kohn, Phys. Rev. **136**, B864 (1964).
[51] A. D. Becke, Phys. Rev. A **38**, 3098 (1988).
[52] C. Lee, W. Yang, and R. G. Parr, Phys. Rev. B **37**, 785 (1988).

[53] R. Parr and W. Yang, *Density-Functional Theory of Atoms and Molecules* (Oxford University Press, Oxford, New York, 1989).
[54] J. Foresman and A. Frisch, *Exploring Chemistry with Electronic Structure Methods* (Gaussian Inc., Pittsburgh, PA, 1996).
[55] M. Dewar, E. Zoebisch, E. Healy, and J. Stewart, J. Am. Chem. Soc. **107**, 3902 (1985).
[56] G. Rocha, R. Freire, A. Simas, and J. Stewart, J. Comput. Chem. **27**, 1101 (2006).
[57] J. Gauss and H. Werner, Phys. Chem. Chem. Phys. **2**, 2083 (2000).
[58] F. London, J. Phys. Radium **8**, 397 (1937).
[59] H. Hameka, Mol. Phys. **1**, 203 (1958).
[60] R. Ditchfield, Mol. Phys. **27**, 789 (1974).
[61] G. Buchanan, G. Montaudo, and P. Finocchiaro, Can. J. Chem. **52**, 3196 (1974).
[62] P. A. Persson, U. Edlund, P. Jacobsson, D. Johnels, A. Soldatov, and B. Sundqvist, Chem. Phys. Lett. **258**, 540 (1996).
[63] C. Goze, F. Rachdi, L. Hajji, M. Núñez-Regueiro, L. Marques, J. L. Hodeau, and M. Mehring, Phys. Rev. B **54**, R3676 (1996).
[64] K. Matsuda, Y. Maniwa, and H. Kataura, Phys. Rev. B **77**, 075421 (2008).
[65] W. Woolfenden and D. Grant, J. Am. Chem. Soc. **88**, 1496 (1966).
[66] A. Hirsch and M. Brettreich, *Fullerenes: Chemistry and Reactions* (Wiley-VCH, Weinheim, 2005).
[67] I. Solov'yov, J. Geng, A. Solov'yov, and B. Johnson, Chem. Phys. Lett. **472**, 166 (2009).